Author Manuscript

Author Manuscript

Author Manuscript

Author Manuscript

HHS Public Access

Author manuscript

Nature. Author manuscript; available in PMC 2018 January 12.

Published in final edited form as:

Nature. 2017 July 20; 547(7663): 360–363. doi:10.1038/nature23010.

Open and Closed Structures Reveal Allostery and Pliability in the HIV-1 Envelope Spike

Gabriel Ozorowski[1,*], **Jesper Pallesen**[1,*], **Natalia de Val**[1], **Dmitry Lyumkis**[2], **Christopher A. Cottrell**[1], **Jonathan L. Torres**[1], **Jeffrey Copps**[1], **Robyn L. Stanfield**[1], **Albert Cupo**[3], **Pavel Pugach**[3], **John P. Moore**[3], **Ian A. Wilson**[1,4], and **Andrew B. Ward**[1]

[1]Department of Integrative Structural and Computational Biology, Center for HIV/AIDS Vaccine Immunology and Immunogen Discovery, International AIDS Vaccine Initiative Neutralizing Antibody Center, and Collaboration for AIDS Vaccine Discovery, The Scripps Research Institute, La Jolla, CA 92037, USA

[2]Laboratory of Genetics and Helmsley Center for Genomic Medicine, The Salk Institute for Biological Studies, 10010 North Torrey Pines Road, La Jolla, CA 92037, USA

[3]Department of Microbiology and Immunology, Weill Medical College of Cornell University, New York, New York, USA

[4]The Skaggs Institute for Chemical Biology, The Scripps Research Institute, La Jolla, CA 92037, USA

SUMMARY

For many enveloped viruses, binding to a receptor(s) on a host cell acts as a first step in a series of events culminating in fusion with the host cell membrane and transfer of genetic material for replication [for review see[1,2]]. The envelope glycoprotein (Env) trimer on the surface of HIV is responsible for receptor binding and fusion. While Env can tolerate a high degree of mutation in five variable regions (V1-V5), and also at N-linked glycosylation sites that contribute roughly half the mass of Env, the functional sites for recognition of receptor CD4 and co-receptor CXCR4/CCR5 are conserved and essential for viral fitness. Soluble SOSIP Env trimers are structural and

Users may view, print, copy, and download text and data-mine the content in such documents, for the purposes of academic research, subject always to the full Conditions of use: http://www.nature.com/authors/editorial_policies/license.html#termsReprints and permissions information is available at www.nature.com/reprints.

Correspondence and requests for materials should be addressed to andrew@scripps.edu.

*these authors contributed equally

Current affiliation and address for N. de Val: NanoImaging Services, 11099 N Torrey Pines Rd Suite 250 La Jolla, CA 92037, USA, nat-deval@hotmail.com.

Author contributions

G.O., N.d.V., D.L., and A.B.W. designed the experiments. G.O., J.L.T., J.C., R.L.S., P.P., and A.C. produced the reagents. N.d.V. prepared cryoEM grids. N.d.V., J.P. and D.L. collected the EM data. D.L. processed the BG505 SOSIP data and J.P. processed the B41 SOSIP data. C.A.C. generated initial homology models. G.O., J.P., and A.B.W. wrote the manuscript. G.O, J.P., N.d.V., J.P.M., I.A.W., and A.B.W. edited the manuscript.

Data availability

CryoEM reconstructions have been deposited in the Electron Microscopy Data Bank under the accession numbers EMD-8713-8717 and EMD-8729-8730. Atomic models of $B41_{b12}$ and $B41_{CD4/17b}$ have been deposited in the Protein Data Bank under accession numbers PDB 5VN8 and 5VN3, respectively.

Competing financial interests

The authors declare no competing financial interests.

Author Manuscript Author Manuscript Author Manuscript Author Manuscript

antigenic mimics of the pre-fusion native, surface-presented Env[3,4], targets of broadly neutralizing antibodies (bnAbs). Thus, they are attractive immunogens for vaccine development [for review see[5–8]]. Here we present high-resolution cryo-electron microscopy (cryoEM) structures of subtype B B41 SOSIP Env trimers in complex with CD4 and antibody 17b, or with antibody b12, at resolutions of ~3.7 Å and ~3.6 Å, respectively, and compare them to cryoEM reconstructions of ligand-free B41 SOSIP Env trimers or in complex with either CD4 or CD4bs antibody PGV04, at ~5.6 Å, ~5.2 Å and ~7.4 Å, respectively. Consequently, we present the most complete description and understanding of the CD4/17b-induced intermediate and provide the molecular basis of the receptor-binding induced conformational change required for HIV-1 entry into host cells. Both CD4 and b12 induce large, previously uncharacterized conformational rearrangements in the gp41 subunits, and the fusion peptide becomes more buried in a newly formed pocket. These structures provide key details on the biological function of the type I viral fusion machine from HIV-1 as well as new templates for inhibitor design.

Numerous biophysical studies have provided a framework for CD4-induced Env conformational changes through a combination of low-resolution cryo-electron tomography of membrane-embedded trimers[9,10], x-ray crystallography of gp120 monomers[11], and more recently hydrogen/deuterium-exchange mass spectrometry (HDX-MS)[12] and Förster resonance energy transfer (FRET)[13] experiments into the dynamics of Env (see Supplementary Discussion for more details). To study the molecular basis of conformational changes resulting from binding of receptor to HIV-1 Env, we obtained a cryoEM map of fully glycosylated B41 SOSIP.664[14] (a solubilized and stabilized version of Env) in complex with two-domain soluble CD4 (sCD4) and the CD4-induced antibody 17b at ~3.7 Å resolution ($B41_{CD4/17b}$) (Fig. 1a; Extended Data Fig. 1; Extended Data Table 1). We also obtained a ~5.6 Å cryoEM map of ligand-free subtype B B41 SOSIP.664 ($B41_{LF}$) and show it to be structurally comparable to subtype A BG505 (Extended Data Fig. 2c–f). Like BG505 SOSIP.664, B41 SOSIP.664 is a stable, native-like trimer that induced autologous neutralizing antibody responses in rabbit immunization studies[15] but can adopt slightly more open conformations (partially open) when analyzed by negative-stain EM, and has a lower melting temperature compared to BG505[14,16] (Extended Data Fig. 2a,b). Despite differences in their biophysical properties, the structure of $B41_{LF}$ (Extended Data Fig. 2f) adopts a closed, pre-fusion conformation nearly identical to the analogous BG505 SOSIP.664 structure (PDB 4ZMJ)[17].

Our structure of $B41_{CD4/17b}$ elucidates the molecular details of receptor-induced conformational changes, including rearrangements of the V1/V2 and V3 loops, and never-seen-before changes in gp41, including repositioning of the fusion peptide (Fig. 1b; SI Video 1). In our $B41_{CD4/17b}$ cryoEM map that contains the complete gp120, most of V1/V2 that extends parallel to CD4 is disordered in the region that was truncated in the core gp120 construct used for crystallography (residues C131 to N187) (Extended Data Fig. 3b). Despite the presence of 17b, whose epitope overlaps the co-receptor binding site, much of the V3 loop beyond the base is also disordered.

CD4/17b binding induces subtle changes in a network of conserved residues (>96% of sequences in the Los Alamos database) in the gp120 core similar to previous observations in

Author Manuscript Author Manuscript Author Manuscript Author Manuscript

gp120 monomers[11,18–20] (Fig. 2a; SI Video 2; Extended Data Table 2). These changes propagate across gp120 to the C1 region (residues 63–72; α0), which is poorly ordered in pre-fusion Env trimer structures (Fig. 1b; Fig. 2c). α0 adopts a stable alpha-helical conformation via transit into a pocket that was sterically occluded by the close juxtaposition of gp120 and HR1 in gp41 in the closed, pre-fusion trimer (Extended Data Fig 3d; SI Video 3). An additional rearrangement of two mannose residues in the D1 arm of the highly conserved N262 glycan into a new pocket underneath the base of V3 further stabilizes the helical conformation of α0 and establishes a direct link between the co-receptor binding site and gp41 (Fig. 2c; Extended Data Fig. 4c). Due to the rotation of gp120, α0 now caps the HR1 helix (α7) of the gp41 subunit from a neighboring protomer, which was previously capped by α1 in gp120 from within a protomer (Fig. 2b). The functional role of α0 that we describe here supports a different conclusion than one based on a recently published low-resolution structure of CD4 bound to an Env trimer in a closed conformation claiming that CD4 makes specific contacts with C1 in the adjacent protomer[21]. In our structure, all of the highly conserved residues claimed to interact with CD4 during its initial pose form intra-gp120 stabilizing interactions in the open CD4-bound structure presented here (Fig. 3d). Mutation of these residues lead to a loss of infectivity[21]; in light of the present work, likely due to destabilization of the conformation competent for co-receptor binding.

Additional cryoEM reconstructions were produced to test the effect of sCD4 alone on Env conformational changes, and compare a with a different Env genotype, BG505 (Extended Data Fig. 1d). Within the limits of resolution we observed only slight differences, whether B41 or BG505 SOSIP was used, and whether 17b is present or not (Extended Data Fig. 3c, Extended Data Fig. 4d). The V3 loop remains unresolved in reconstructions of B41 or BG505 SOSIP in complex with sCD4, suggesting that sCD4 alone is responsible for the gp120 rearrangements and exposure of the co-receptor site, and suggesting that 17b does not induce further conformational changes (Extended Data Fig. 4f).

VRC01-class antibodies[22] bind the CD4bs but do not induce global conformational changes in the Env trimer while another CD4bs neutralizing antibody, b12, has been shown to engage Env in a different manner[9,14,23]. To better understand the conformational changes induced by b12, we generated cryoEM structures of B41 SOSIP.664 in complex with either CD4bs antibody PGV04 ($B41_{PGV04}$) or b12 ($B41_{b12}$) to resolutions of ~7.4 Å and ~3.6 Å, respectively (Fig. 4a; Extended Data Fig. 1; Extended Data Fig. 5a, c). While $B41_{PGV04}$ was nearly identical to BG505 SOSIP.664 in complex with VRC01-like antibodies, $B41_{b12}$ promoted a large-scale change in Env away from the closed pre-fusion conformation similar to $B41_{CD4/17b}$ (Extended Data Fig. 5b, d, e). Specifically, $B41_{b12}$ exhibits a large rigid body movement of all three gp120 subunits with respect to the trimer axis and concomitant rearrangement of the gp41 helices (discussed below) (Fig. 4c; Extended Data Fig. 5d). Despite the gp120 rearrangements, the V3 loop remains sequestered beneath V1/V2 and the co-receptor binding site is inaccessible (Fig. 4b; Extended Data Fig. 6b). Thus, while b12 makes similar interactions with Env as CD4 it does not induce a conformational change in V1/V2 relative to gp120 (Fig. 4b; Extended Data Fig. 4e). Notably, the subtle rearrangement of mannose residues in the N262 glycan observed in $B41_{CD4/17b}$ is not seen in $B41_{b12}$, and density for the α0 region is highly disordered. Thus, functional progression of the Env requires both a rigid body movement of gp120 and CD4-induced allosteric changes within

Author Manuscript Author Manuscript Author Manuscript Author Manuscript

gp120 to expose the co-receptor binding site. Unlike CD4, b12 is sterically occluded from binding the closed pre-fusion conformation of Env (Extended Data Fig. 4b; Extended Data Fig. 6c–f), suggesting that transient opening of the trimer is required for b12 epitope exposure. Upon binding, b12 prevents reversion back to the closed pre-fusion state (Extended Data Fig. 6d).

Globally, both CD4/17b and b12 result in gp41 rearrangements that, in the case of the former, prime for further transitions to facilitate fusion with the host-cell membrane. The HR1 three-helical bundle begins to open up at the base, causing the N-terminal half of the HR1 peptide ($HR1_N$) to move away from the center of the trimer (Extended Data Fig. 7g). This movement coincides with formation of a stable helix in the fusion peptide proximal region (FPPR) and $HR1_N$ that packs against HR2 (Extended Data Fig. 7h). Additionally, gp120 C1 (V36-P43) and C5 (starting at I491) regions undergo a similar movement in the same direction to avoid clashing with α9b of HR2. Finally, HR2 tilts upward and, when modeled onto the surface of a virion, would be more perpendicular to and somewhat lifted off the membrane compared to the pre-fusion state.

One of the major consequences of the movement of gp120 relative to gp41 is the formation of a new pocket close to the trimer core that, in $B41_{b12}$ and $B41_{CD4/17b}$, houses the fusion peptide (FP). FP, which is fully resolved to the N-terminal residue A512 in $B41_{b12}$ and L515 $B41_{CD4/17b}$, undergoes a large conformational rearrangement upon entry into this pocket (Fig. 3a, e; Extended Data Fig. 7c–e; SI Video 4), and is stabilized by many newly formed interactions. For example, K574, which forms a salt bridge with D107 of gp120 in the closed pre-fusion state, undoes this interaction upon translocation of α1 induced by CD4/17b-binding, but forms a cation-π interaction with gp120 F53 (Fig. 3b; Extended Data Fig. 7a). All three residues (F53, D107, K574) are >99% conserved and the interplay between them likely contributes to two stable states (Extended Data Table 2). In fact, mutational analysis demonstrates that introduction of an F53A mutation not only decreases infectivity but also leads to greater gp120 shedding[18,24]. The gp120 interface with gp41 α7 in $B41_{CD4/17b}$ is further stabilized by highly conserved residues that do not make any productive interactions in the pre-fusion state (Fig. 3b). Finally, despite the larger conformational change, conserved phenylalanine residues in the FP and FPPR provide additional stabilizing interactions (Fig. 3e). In addition to formation of new contacts, the intermediate state exemplified by $B41_{CD4/17b}$ also retains some stabilizing features of the closed pre-fusion state (Fig. 3c; Extended Data Fig. 7f). Altogether, this extensive network of interactions between highly conserved residues suggests that the CD4/17b-bound state represents a stable, fusion intermediate wherein the fusion peptide is embedded inside the trimer distant from the host membrane and therefore requiring further triggering by co-receptor engagement.

The Env trimer on the surface of HIV must maintain a fine balance between stability until a target cell is reached and the ability to trigger and undergo conformational rearrangement that drives fusion. Our studies describe Env, even when stabilized by SOSIP mutations, as a dynamic molecule that fluctuates between closed and open pre-fusion states. In the open conformation, we now see that the FP is structured and sequestered near the core of the trimer. We hypothesize that the FP may transition between solvent-exposed and sequestered conformations based on “breathing” in the trimer. The structure of FP in our b12- or

Author Manuscript Author Manuscript Author Manuscript Author Manuscript

CD4/17b-bound structures could therefore be used to inform structure-based design of stabilized or cyclic fusion peptide mimetic inhibitors of HIV[25,26].

Finally, we show that CD4bs neutralizing antibodies can prevent exposure of the co-receptor binding site in both the open (e.g. b12) or closed conformation (e.g. VRC01) by restricting movement of the V1/V2 loops (Extended Data Fig. 8). CD4, on the other hand, induces a series of allosteric changes that propagate across gp120 and expose the co-receptor binding site. While the co-receptor binding site is accessible in the CD4-bound structure, it is unclear how further conformational changes in the trimer are triggered by interaction with CCR5/CXCR4, although the glycan at N262 and formation of α0 likely play a role in signal transmission. Based on the disposition of the co-receptor binding sites three copies of CCR5[27] could bind to the trimer in this conformation. Interestingly, CCR5 forms a crystallographic dimer in the x-ray structure[27] that when docked on top of our trimer structure spans across two gp120 subunits and could potentially interact with two co-receptor binding sites simultaneously (Extended Data Fig. 8). Overall, our structural studies have unlocked the molecular details of the first step in the CD4 receptor-mediated fusion process of Env, but the role of the co-receptor remains to be elucidated.

Methods

Protein expression

BG505 SOSIP.664 and B41 SOSIP.664 trimers were expressed by transient transfection (co-transfected with furin) in HEK293F (Invitrogen; mycoplasma-free) and purified as previously described using 2G12-affinity and size-exclusion chromatography[28,29].

The two N-terminal domains of human CD4 were cloned into vector pHCMV3 with an N-terminal Ig-kappa secretion signal and a C-terminal hexahistidine tag for expression in HEK293F. One liter of 293 Freestyle cells was transiently transfected with 0.5 mg of DNA. After 7 days, the supernatant containing the secreted protein was applied to a 5ml HisTrap FF column (GE Healthcare) at 1 ml/min. The protein was eluted with a gradient from 0–100% of 1.5 M glycine in 0.02 M Tris-acetate pH 8.0, and 0.5 M NaCl. Peaks containing CD4 (as verified by SDS-PAGE) were pooled and further purified by size exclusion chromatography on an S75 16/60 column (GE Healthcare) in 0.05 M Tris-acetate pH 8.0 and 0.3 M NaCl.

PGV04, 17b or b12 Fab was expressed in HEK293F and purified by 5 mL KappaSelect or LambdaSelect affinity (GE Healthcare), MonoS 5/50 GL (GE Healthcare), and Superdex 200 Increase 10/300 GL (GE Healthcare).

Sample preparation

BG505 SOSIP.664 were mixed with a 10X molar excess (sCD4:trimer) of sCD4 for 2 hr at room temperature. For complexes containing 17b, a subsequent incubation was performed with a 10X molar excess (Fab:trimer) of 17b Fab for 1 hr at room temperature. The complex was purified by size exclusion chromatography (SEC) using Superose 6 10/300 GL (GE Healthcare) in TBS (0.05 M Tris pH 7.4, 0.15 M NaCl). The fractions containing the complex were pooled and concentrated using a 100-kDa concentrator (Amicon Ultra,

Author Manuscript Author Manuscript Author Manuscript Author Manuscript

Millipore) to ~40 μL at 1 mg/mL. 5 μL of the complex was incubated with 3 μL of a fresh DDM solution at 1.8 mM. A 3 μL aliquot of the complex was applied to a C-Flat grid (CF-2/2-4C, Electron Microscopy Sciences, Protochips, Inc.) which had been plasma cleaned for 5 seconds using a mixture of Ar/O2 (Gatan Solarus 950 Plasma system), blotted off, and then immediately plunged into liquid ethane using a manual freeze plunger.

The same procedure was used to prepare the B41 complexes except that the incubation time of trimer and ligand(s) was increased to ~18 hrs prior to SEC. This long incubation time increased stoichiometry of binding for ligands with slow on-rates and did not have an effect on overall trimer stability judged by the lack of dimers or monomers in both SEC peaks and EM classifications.

CryoEM data collection

Frozen-hydrated samples were inserted into a Titan Krios electron microscope (FEI, Hillsboro, Oregon) operating at 300 kV. Data was collected through the Leginon software solution[30–32]. Each micrograph movie was collected at a magnification of 22,500, which resulted in a pixel size of 1.31 Å in the specimen plane. Micrograph movies were acquired using a K2 direct detector camera (Gatan, Pleasanton, California) operated in counting mode with 200 ms exposure per frame. Dose rate was ~10 e-/pix/sec and defocus range was −1.0 to −4.0 μm. Micrograph movie frames were aligned and dose-weighted using MotionCor2[33]. CTF models were calculated using GCTF[34].

Data processing for $B41_{LF}$, $B41_{b12}$, $B41_{PGV04}$, and $B41_{CD4/17b}$

Molecular projection image candidates were then identified in the aligned micrograph movies using DoG Picker[35]. Reference-free, 2D classification was performed using identified projection image candidates binned by a factor of two via iterative multivariate statistical analysis and multi-reference alignment[36,37]. Particles corresponding to class averages of the molecular complexes were selected for further processing in Relion version 2.0[38]. Initially, full-size molecular projection images were refined against a simulated density map of an unliganded BG505 SOSIP Env trimer (simulated from the Env part of PDB ID 5CEZ) low-pass filtered at 60 Å. Initial refinement was followed by 3D classification and stable symmetrical classes were selected for further symmetrized (C3) refinement. Resolutions were calculated using soft-edged masks that encompassed the entire structure (including all noisier regions) and are reported according to the FSC 0.143 gold-standard criterion. Final resolutions are ~3.6 Å ($B41_{b12}$), ~3.7 Å ($B41_{CD4/17b}$), ~5.2 Å ($B41_{CD4}$), ~5.6 Å ($B41_{LF}$) and ~7.4 Å ($B41_{PGV04}$).

Data processing of $BG505_{sCD4}$ and $BG505_{sCD4/17b}$

Single particles were selected using DoGPicker[35] from the whole-frame aligned and summed micrographs and used to create an initial raw particle stack after removing regions of the micrographs containing gold or large areas of aggregation. The raw particle stack was extracted using a box size of 256 pixels, and was immediately binned by 2 in reciprocal space, to a pixel size of 2.62 Å/pix and a box size 128 pixels. Initial 2D classification in Relion indicated a mixture of particle populations from sub-stoichiometric binding of sCD4 and 17b. Particles contributing to classes that did not produce clear structural features were

Author Manuscript Author Manuscript Author Manuscript Author Manuscript

discarded, leaving 98,845 particles. Next, to separate the different particle populations, this stack was subjected to competitive sorting using 3 initial models – trimer alone, trimer + sCD4, trimer + sCD4 + 17b Fab – in an identical manner as previously described[39]. This resulted in three separate stacks containing 69,105 particles (trimer alone), 6,342 particles (trimer + sCD4), and 23,398 particles (trimer + sCD4 + 17b). Each of these individual stacks was then subjected to 4-model classification in Relion, using 60 Å as the initial low-pass filter value[38], followed by parameter conversion and final classification in Frealign[40]. For each subgroup, the number of classes in Frealign was varied from 2 to 4, and a final value was selected such that the classification would produce at least 2 nearly identical models, as described earlier[41,42]. Within the stack comprising the trimer alone or the trimer + sCD4, this procedure resulted in removal of bad particles that did not produce interpretable maps (Figure S5C); within the stack comprising the trimer + sCD4 + 17b, this resulted in 1 low resolution class that was discarded, as well as 3 classes that differed in the relative configuration of the 17b Fab, but that were otherwise very similar. Final resolutions (FSC 0.143) are ~10.5 Å ($BG505_{CD4}$), and ~8.6 Å ($BG505_{CD4/17b}$).

Model building and refinement

Model building and refinement steps followed those previously described[43]. Briefly, initial homology models of B41 gp120 and gp41 were generated using Modeller[44] and the crystal structure of ligand-free BG505 SOSIP.664 (PDB: 4ZMJ) as a template for $B41_{LF}$ and $B41_{b12}$, while the crystal structure of gp120 bound to sCD4 and 17b (PDB: 1GC1) was used to model gp120 of $B41_{CD4/17b}$. Coordinates for sCD4, 17b, b12, and PGV04 were obtained from PDB IDs 1GC1, 1RZ8, 2NY7, and 3J5M, respectively. Individual chains were fit into the respective cryoEM maps using UCSF Chimera[45] and refined using a combination of Rosetta density-guided iterative local refinement[46], RosettaRelax[47], and manual building in COOT[48]. Glycans were built using an idealized Man9 model that was placed into corresponding glycan density in UCSF Chimera. Torsion angles were adjusted in UCSF Chimera until good agreement was achieved between map and model. Sugar molecules with disordered or no density were removed. The final models were further refined using Phenix[49] real space refinement without NCS constraints. Glycans were validated by pdb-care[50] and CARP[51] and structures were evaluated using EMRinger[52] and Molprobity[53]. Figures were generated in UCSF Chimera or Pymol[54]. Buried surface area calculations were performed using PDBePISA[55] and R.M.S.D. analysis was performed in UCSF Chimera. Map fitting cross correlations were calculated using the Fit In Map feature in UCSF Chimera.

Negative stain EM

A stock of B41 SOSIP.664 was thawed on ice and 3 μL were adsorbed onto a Cu400 carbon-coated grid for 10 s before blotting, and then stained for 60 s with 2% (w/v) uranyl formate. The remaining stock was then incubated at 37°C for 1 hr on a heat block. 3 μL were removed and immediately adsorbed onto a carbon-coated grid followed by staining. The stock was again incubated on ice for 1 hr before a third grid was prepared using the same method. Data were collected and processed as described in Pugach et al., and de Taeye et al.

Author Manuscript Author Manuscript Author Manuscript Author Manuscript

Extended Data

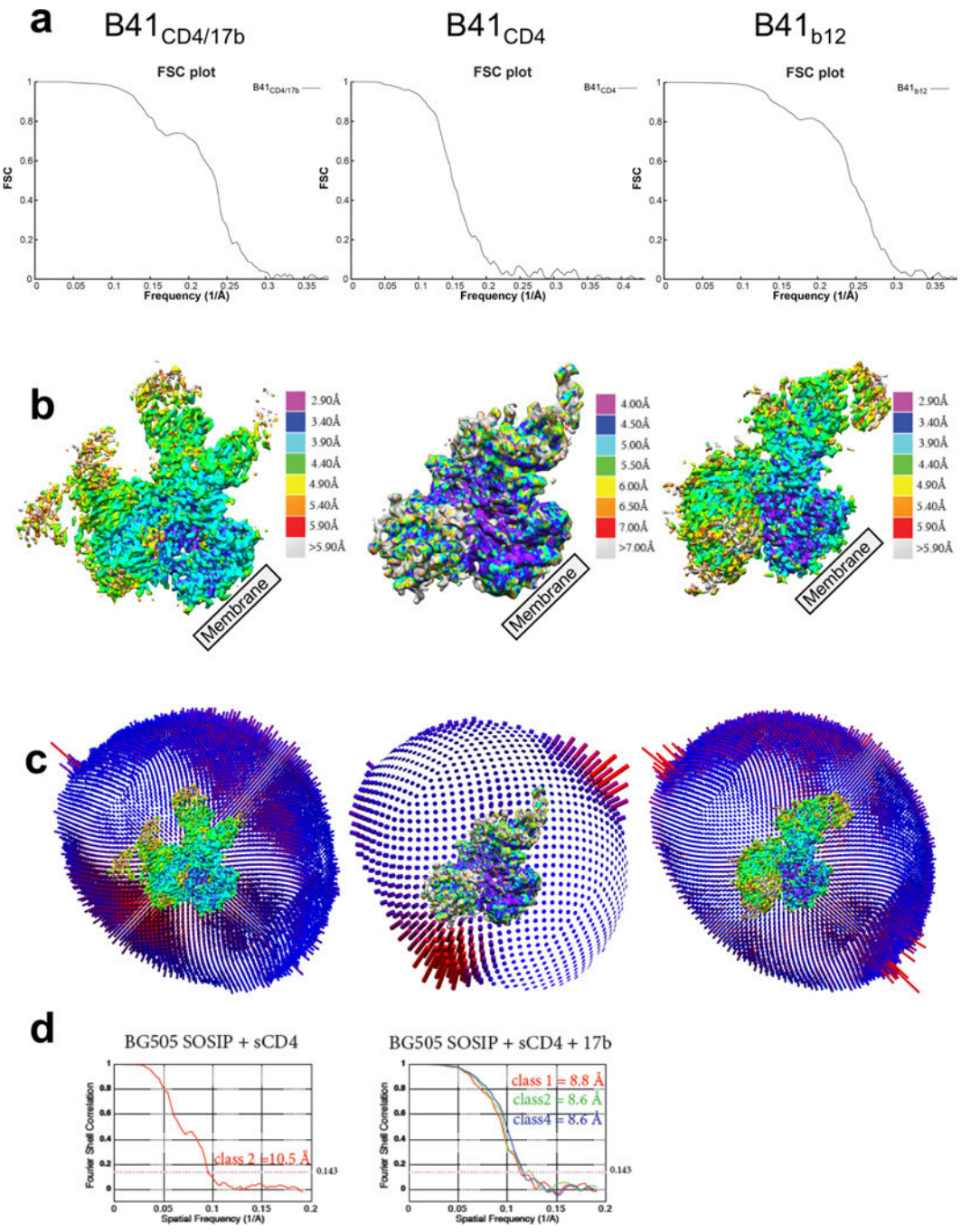

Extended Data Figure 1. CryoEM statistics of $B41_{CD4}$, $B41_{CD4/17b}$ and $B41_{b12}$

(**a**) Fourier shell correlations. (**b**) Local resolution estimates. (**c**) Angular distribution plots. (**d**) Fourier shell correlations for $BG505_{CD4}$ and $BG505_{CD4/17b}$.

Author Manuscript Author Manuscript Author Manuscript Author Manuscript

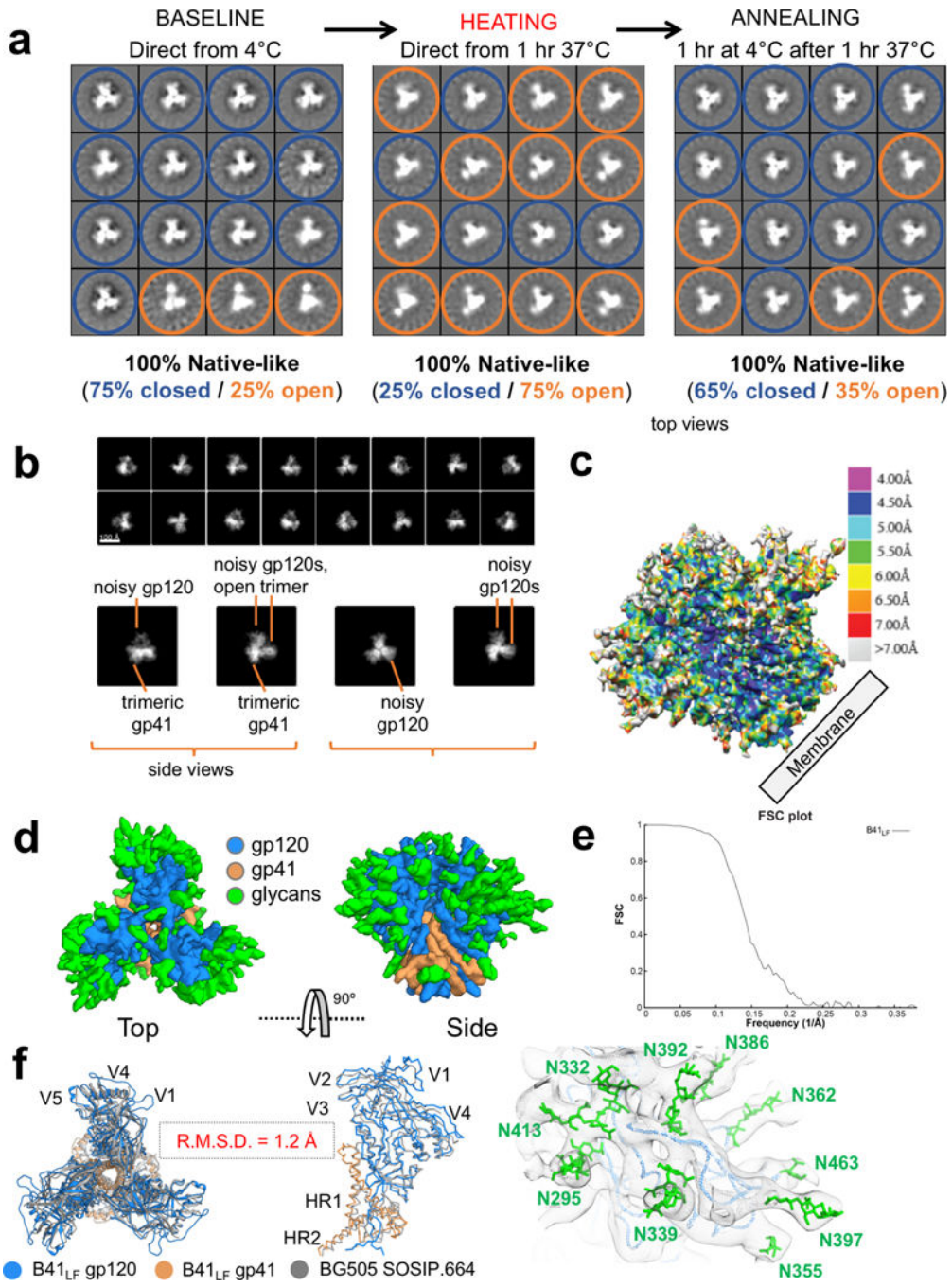

Extended Data Figure 2. Cryo-EM reconstruction of ligand-free B41 SOSIP.664

(**a**) The "breathing" of B41 SOSIP.664 trimers is suggested by negative-stain 2D class averages with representative open (blue) and closed (orange) phenotypes highlighted. Sample temperature influences the percentage of open and closed phenotypes, and the open state is reversible. (**b**) CryoEM 2D class averages also suggest flexibility of the gp120 subunits relative to one another as evidenced by the blurring of gp120s in the class averages. (**c**) CryoEM reconstruction colored by local resolution for $B41_{LF}$. (**d**) The segmented cryoEM map colored by component (gp120, gp41, glycans). The top view is defined as

looking towards the viral membrane. (**e**) Fourier shell correlation (FSC) for $B41_{LF}$. (**f**) Superposition of the x-ray structure of ligand-free BG505 SOSIP.664 (PDB 4zmj) onto a homology model of B41 SOSIP.664 refined into the cryoEM map (Cα R.M.S.D. ~1.2 Å). All three protomers are presented in the top view (*left*), while only a single protomer is shown in the side view for clarity (*middle*). Displayed is the V4 region and surrounding glycans (*right*).

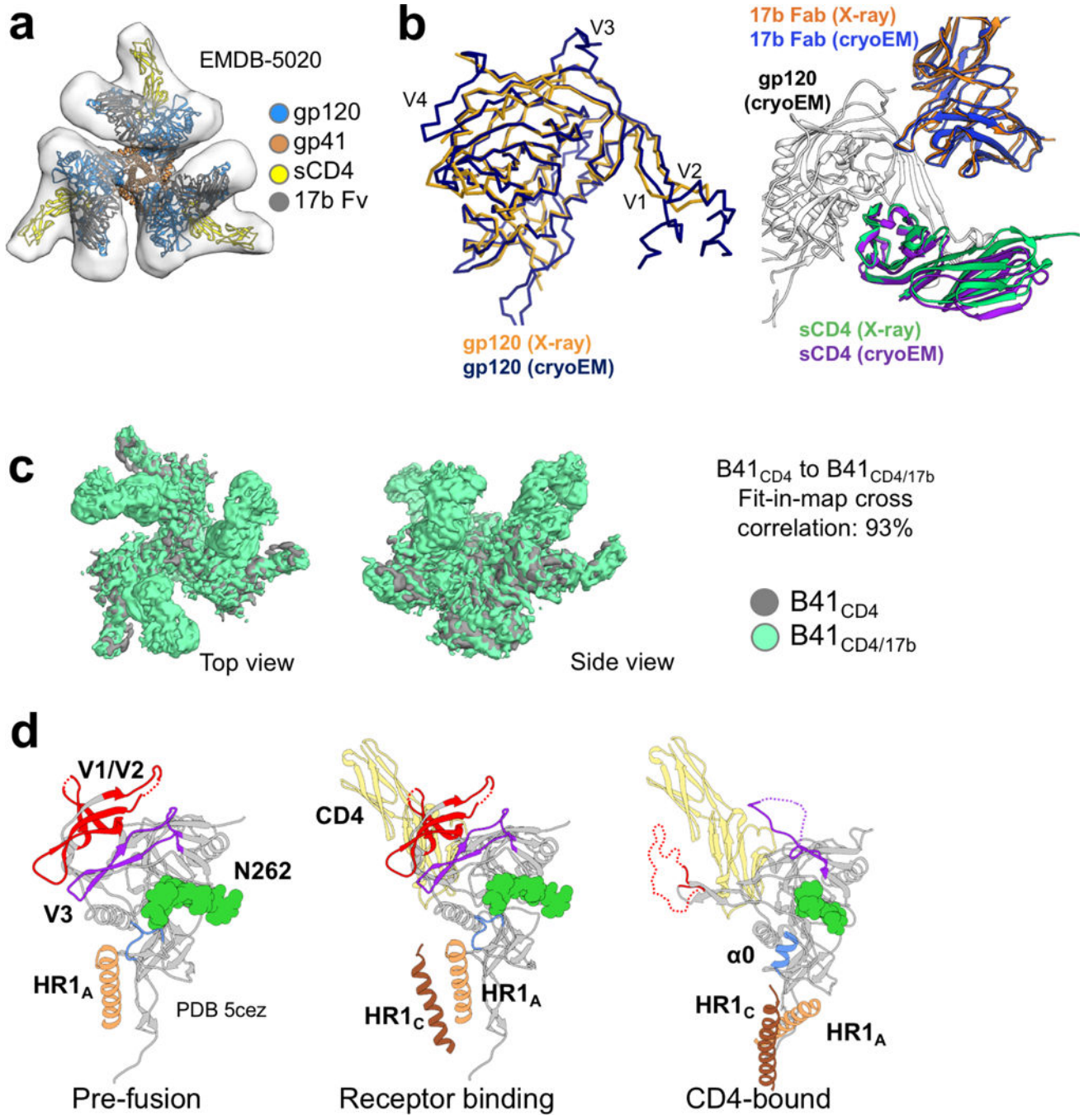

Extended Data Figure 3. Comparison of $B41_{CD4/17b}$ model

Author Manuscript Author Manuscript Author Manuscript Author Manuscript

Author Manuscript Author Manuscript Author Manuscript Author Manuscript

(**a**) Fitting of the cryoEM $B41_{CD4/17b}$ model into a cryoET reconstruction of surface-expressed Env in complex with sCD4 and 17b. (**b**) Alignment of gp120 in complex with CD4 and 17b from the cryoEM and x-ray crystallography models (PDB 1gc1). The Cα R.M.S.D. between our model and the x-ray structure of gp120 core in complex with sCD4 and 17b (PDB 1gc1) is ~1.5 Å, which is relatively low considering only 79% identity between the BG505 and B41 Env sequences. (**c**) Map fitting of $B41_{CD4}$ into $B41_{CD4/17b}$ (low pass filtered to 5.2 Å) results in a cross correlation of 93%. (**d**) Cartoon representation of the major changes involved in the formation of the α0 helix. Pre-fusion model based on PDB 5CEZ.

Author Manuscript Author Manuscript Author Manuscript Author Manuscript

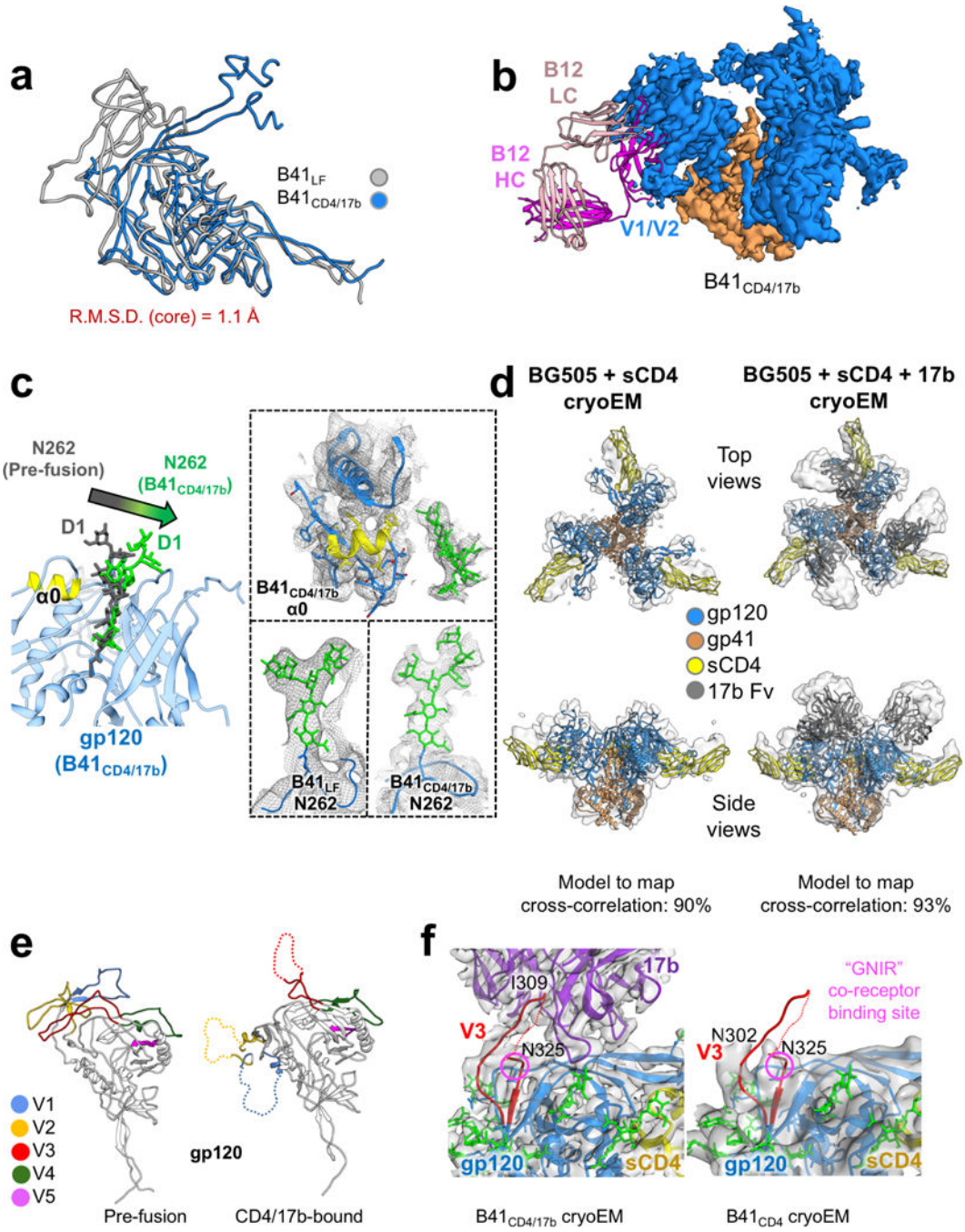

Extended Data Figure 4. Conformational differences between pre-fusion, b12-bound, and CD4-bound state

(**a**) Alignment of gp120 from the cryoEM models of $B41_{LF}$ and $B41_{CD4/17b}$ illustrates a significant displacement of the V1, V2, and V3 loops. (**b**) Fitting of the $B41_{b12}$ model into the map of $B41_{CD41/17b}$ reveals a steric barrier created by b12 that prevents the translocation of V1/V2, which would clash with the antibody heavy chain. (**c**) Glycan N262 is repositioned away from the C1 domain of gp120 upon sCD4 binding as a result of V3 translocation (*left*). The relative positions of N262 in $B41_{LF}$ and $B41_{CD4/17b}$ are supported

Author Manuscript Author Manuscript Author Manuscript Author Manuscript

by continuous density (*right*). (**d**) Comparison of the cryoEM model of $B41_{CD4/17b}$ to cryoEM reconstructions of $BG505_{CD4}$ and $BG505_{CD4/17b}$. (**e**) Relative movements of variable loops between pre-fusion and CD4-bound states of B41 SOSIP (*left*). Loss of density for the V3 loop in both $B41_{CD4}$ and $B41_{CD4/17b}$ maps suggests that V3 movement is in response to priming by CD4 and not caused by 17b or the co-receptor (*right*).

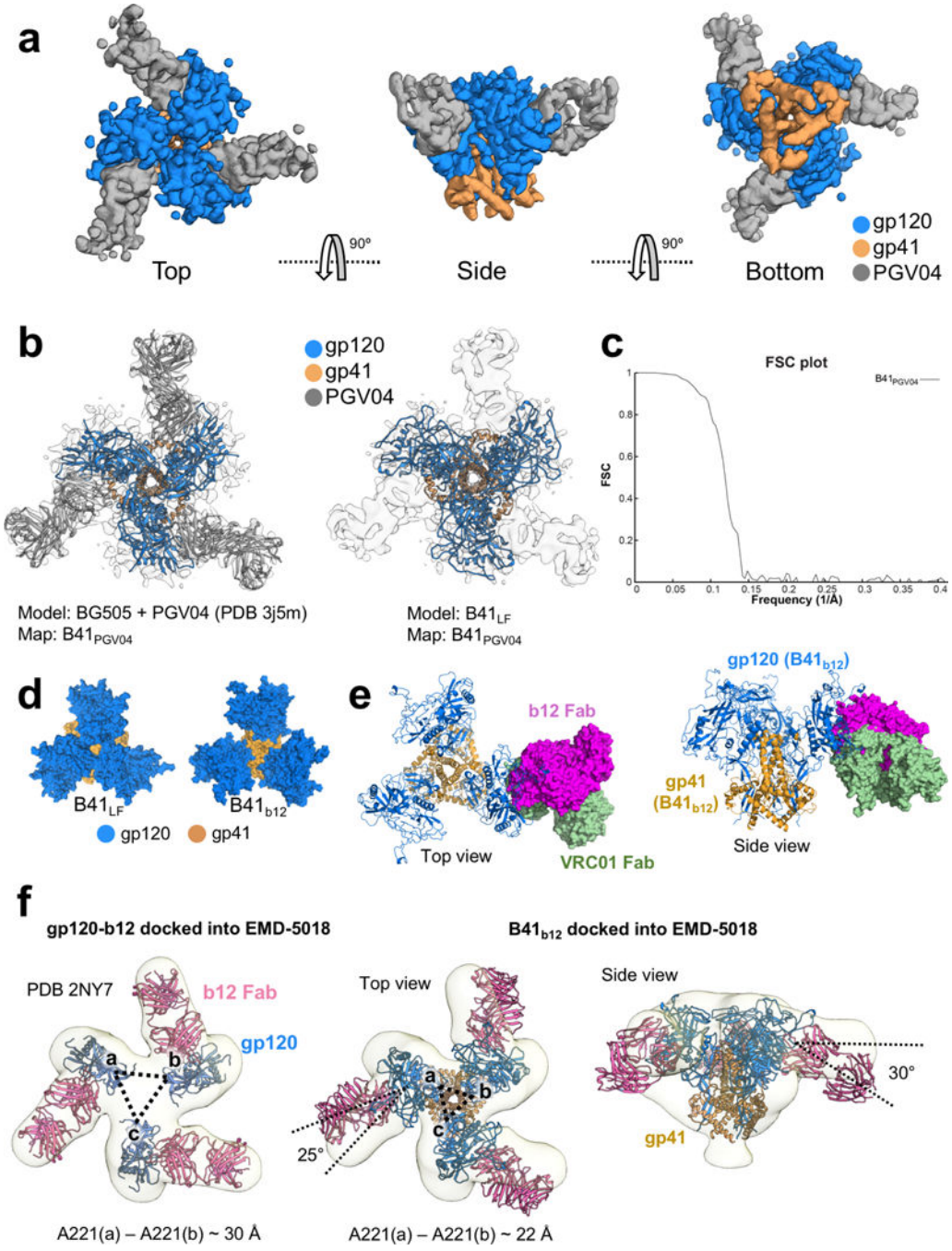

Extended Data Figure 5. CryoEM reconstruction of B41 SOSIP.664 in complex with PGV04 Fab

Author Manuscript Author Manuscript Author Manuscript Author Manuscript

(**a**) Segmented cryoEM map with components colored according to the key. (**b**) Docking of BG505 + PGV04 (PDB 3J5M) and $B41_{LF}$ models into the B41 + PGV04 reconstruction. Comparison with BG505 bound to PGV04 demonstrates a high degree of structural similarity (91% correlation between the two cryoEM maps), and docking of the $B41_{LF}$ model into the $B41_{PGV04}$ map results in excellent agreement, with the $B41_{LF}$ backbone atoms falling into density as well as alignment of PNGS asparagine residues with glycan density (94% correlation between $B41_{LF}$ and $B41_{PGV04}$ maps). (**c**) FSC of $B41_{PGV04}$. (**d**) gp120 rotation and movement away from the central axis in the b12-bound state. (**e**) Comparison of VRC01 and b12 epitopes with respect to the open, b12-bound conformation of B41 SOSIP.664. (**f**) Docking of either the crystal structure of gp120-b12 or the $B41_{b12}$ cryoEM model into the ECT reconstruction of HIV-1 BaL in complex with b12 (EMDB-5018) reveals differences in relative movement and rotation of gp120 from the trimer axis and ultimate position of b12.

Author Manuscript Author Manuscript Author Manuscript Author Manuscript

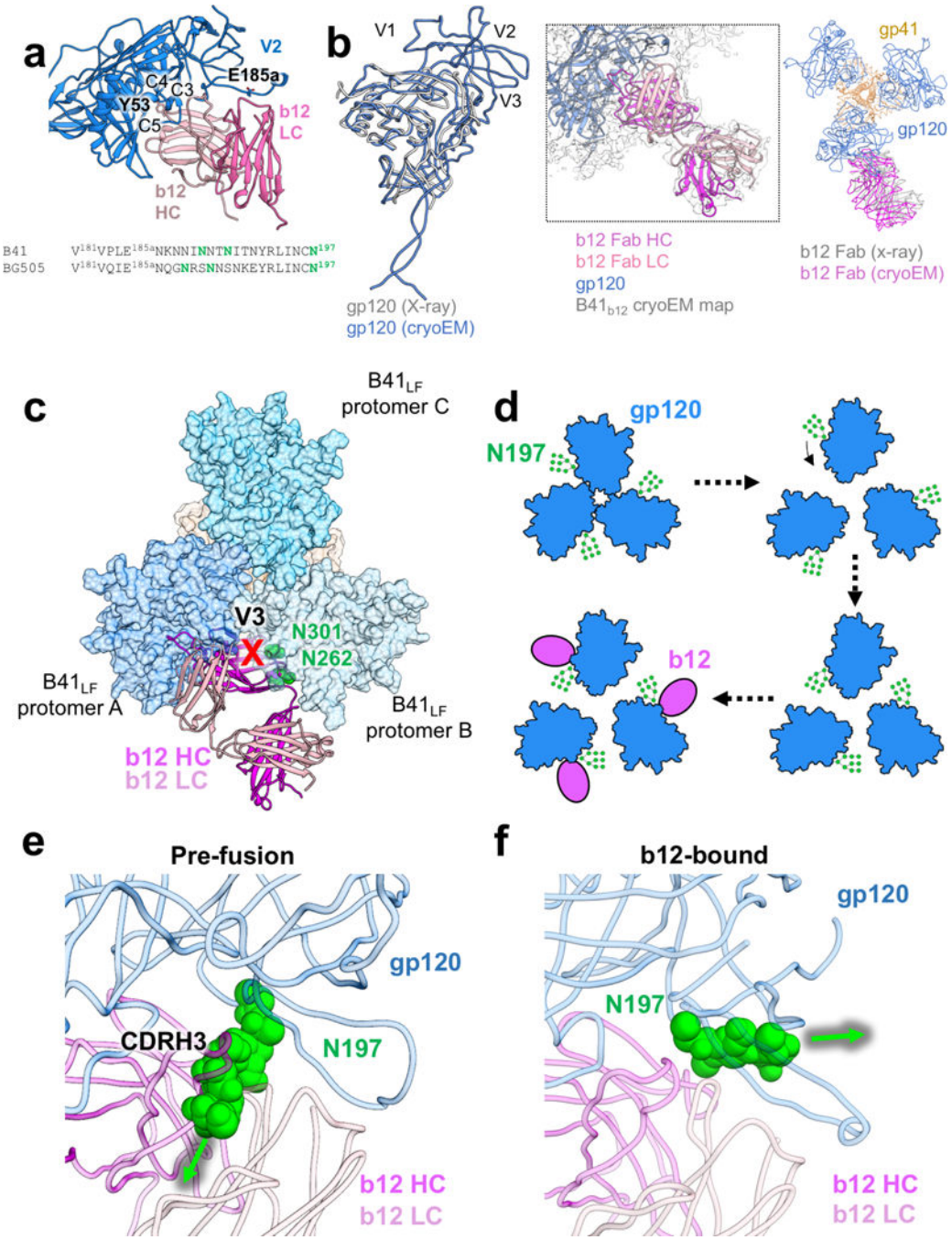

Extended Data Figure 6. Comparison of the B41$_{b12}$ cryoEM model to the x-ray model of gp120 in complex with b12 Fab, and glycan repositionin

(**a**) Major contacts between b12 Fab and gp120 highlighted based on the cryoEM model. Sequence alignment between BG505 and B41 Env for a segment of V2, with N-linked glycans colored green. (**b**) Alignment of gp120 in complex with b12 from the cryoEM and x-ray crystallography models (PDB 2NYZ) (*left*). The crystal structure of b12 Fab docked into the B41$_{b12}$ cryoEM map, revealing that the elbow angle is preserved (*middle*). When aligned to gp120, the x-ray model reveals a slightly different b12 angle of approach with

Author Manuscript Author Manuscript Author Manuscript Author Manuscript

respect to the cryoEM model (*right*). These differences may arise due to a more stable, neutralization resistant Tier-2 virus (B41) versus a more flexible lab-adapted Tier 1 BaL pseudovirus, the stabilizing SOSIP modifications used in the soluble constructs (although none are located at the CD4bs epitope or gp120 core), or the low resolution of the cryoET map. (**c**) The pre-fusion arrangement of gp120 does not allow for b12 binding to B41 SOSIP.664 due to clashes between the framework regions of the antibody and portions of a neighboring gp120 monomer (V3 and glycans). (**d**) Rotation of the N197 glycan requires the gp120 subunits to open up and move away from one another. (**e,f**) Glycan N197 in the b12 epitope acts as a steric barrier in the pre-fusion state and rearranges and moves away from the b12 epitope to allow for b12 binding.

Author Manuscript Author Manuscript Author Manuscript Author Manuscript

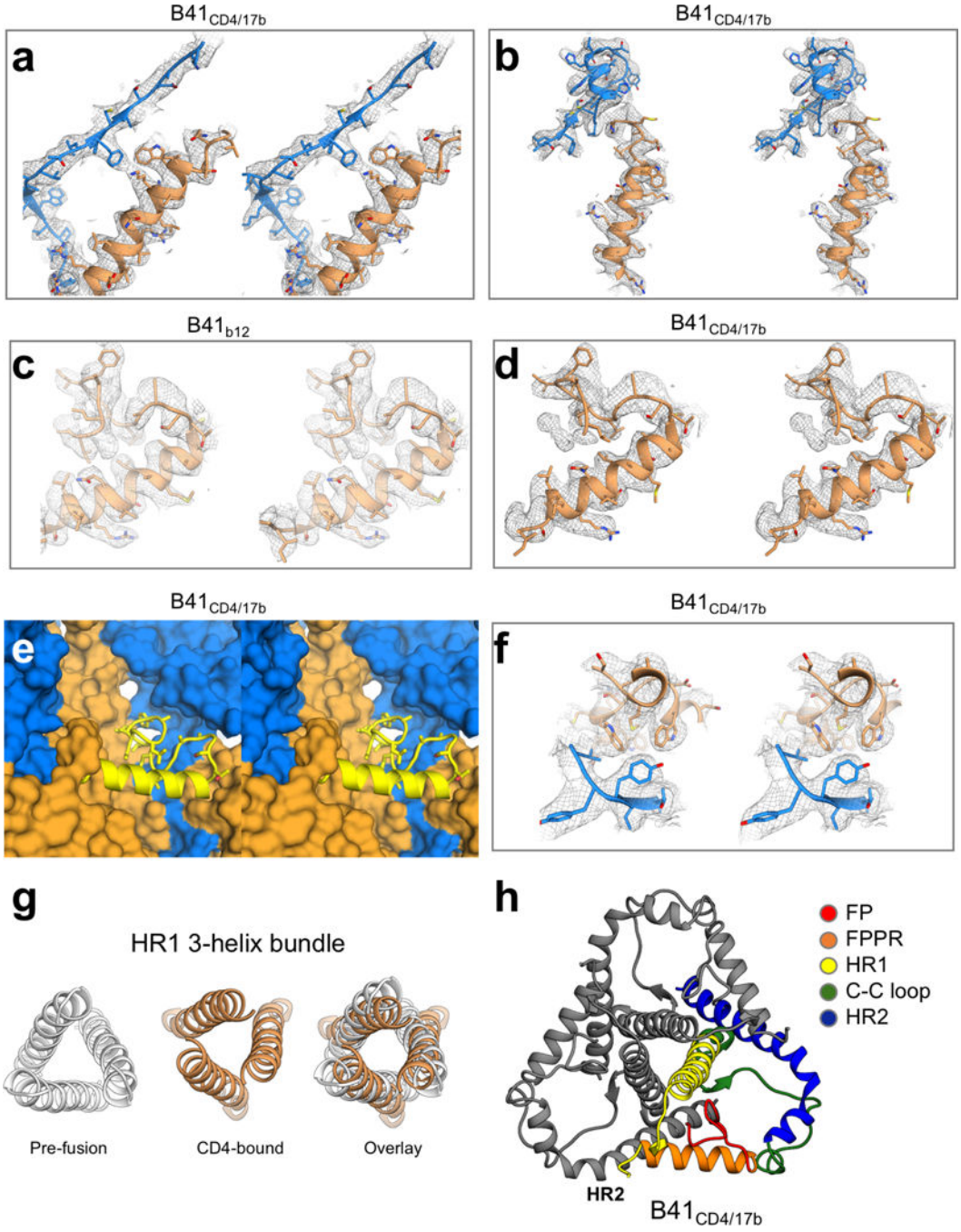

Extended Data Figure 7. CryoEM density of various stabilizing interactions in B41$_{CD4/17b}$

(**a, b**) Stereo images of cryoEM density of specified contour levels for **(a)** K574-D107, and **(b)** the α0 HR1 cap of B41$_{CD4/17b}$. (**c, d**) Fusion peptide and fusion peptide proximal region electron density for (**c**) B41$_{b12}$ and (**d**) B41$_{CD4/17b}$. (**e**) Stereo image of pocket protecting the fusion peptide in the CD4-bound state. (**f**) Stereo image of electron density of the Trp clasp region in B41$_{CD4/17b}$. (**g**) HR1 3-helix bundle rearrangement between pre-fusion and CD4-bound states. (**h**) gp41 arrangement in B41$_{CD4/17b}$. The FPPR and HR1$_N$ pack against regions of HR2 from two different protomers.

Author Manuscript Author Manuscript Author Manuscript Author Manuscript

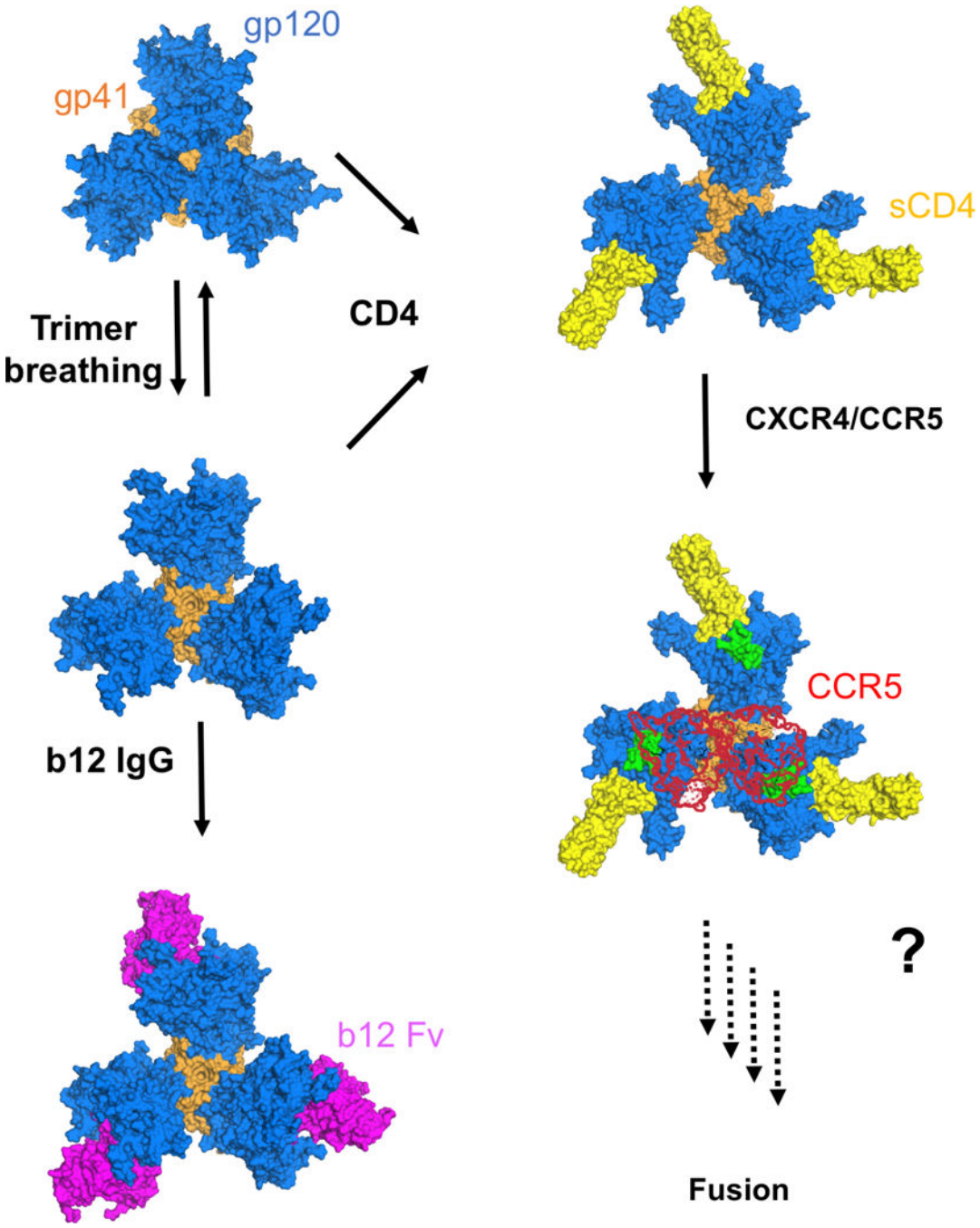

Extended Data Figure 8. Overview of HIV-1 Env conformational states

Various biophysical data strongly suggest that the pre-fusion trimer is in an equilibrium of reversible open and closed states. b12 recognizes a more open state and traps the trimer in an irreversible intermediate state that can no longer play a role in host cell fusion. CD4, on the other hand, induces a stable, fusion intermediate that displays the co-receptor binding site and primes the fusion peptide to move to a more centralized location in the trimer interface. It is only after binding of CXCR4/CCR5 to CD4-bound Env that additional fusion steps occur, highlighted by the full formation of a three-helix bundle before final condensation

Author Manuscript Author Manuscript Author Manuscript Author Manuscript

into a six-helix bundle. When a dimer of CCR5 from a crystal structure is docked on top of the trimer structure, the N-termini of the two co-receptors are situated proximal to the co-receptor binding sites on gp120.

Extended Data Table 1

CryoEM and model refinement statistics.

Map	B41_b12	B41_CD4_17b	B41_LF	B41_CD4	B41_PGV04
Data collection					
Microscope	FEI Titan Krios	FEI Titan Krios	FEI Titan Krios	FEI Talos Arctica	FEI tecnai G2 F20
Voltage (kV)	300	300	300	200	200
Detector	Gatan K2 Summit	Gatan K2 Summit	Gatan K2 Summit	Gatan K2 Summit	Gatan K2 Summit
Recording mode	Counting	Counting	Counting	Counting	Counting
Magnification (incl. post-magnification)	38,168	38,168	38,168	43,478	41,322
Movie micrograph pixelsize (Å)	1.31	1.31	1.31	1.15	1.21
Dose rate (e*/[(camera pixel)*s])	10	10	10	8.6	10
Number of frames per movie micrograph	50	50	35	50	25
Frame exposure time (ms)	200	200	200	200	200
Movie micrograph exposure time (s)	10	10	7	10	5
Total dose (e*/Å2)	58	58	41	65	34
Defocus range (μm)	1.0–4.0	1.0–4.0	1.0–4.5	0.8–2.5	1.0–4.5
EM data processing					
Number of movie micrographs	1,300	1,169	2,042	1,540	1,517
Number of molecular projection images in map	88,071	46,855	42,541	46,567	9,475
Symmetry	C3	C3	C3	C3	C3
Map resolution (FSC 0.143; Å)	3.6	3.7	5.6	5.2	7.4
Map sharpening B-factor (Å2)	−124	−124	−250	−231	−533
Structure Building and Validation					
Number of atoms in deposited model					
gp120	10,341	9,150	n/a	n/a	n/a
gp41	3,312	3,270	n/a	n/a	n/a
b12	5,547	n/a	n/a	n/a	n/a
17b	n/a	5,514	n/a	n/a	n/a
SCD4	n/a	4,113	n/a	n/a	n/a
glycans	1,551	1,689	n/a	n/a	n/a
MolProbity score	1.92	1.93	n/a	n/a	n/a
Clashscore	5.54	6.27	n/a	n/a	n/a
EMRinger score	2.44	2.38	n/a	n/a	n/a
RMSD from ideal					
Bond length (Å)	0.010	0.010	n/a	n/a	n/a
Bond angles (*)	1.13	1.18	n/a	n/a	n/a
Ramachandran plot					
Favored (%)	86.95	88.80	n/a	n/a	n/a

Author Manuscript Author Manuscript Author Manuscript Author Manuscript

Map	B41_b12	B41_CD4_17b	B41_LF	B41_CD4	B41_PGV04
Allowed (%)	12.42	10.76	n/a	n/a	n/a
Outliers (%)	0.63	0.43	n/a	n/a	n/a
Average B-factor	72	92	n/a	n/a	n/a

Extended Data Table 2

Conservation of key amino acids based on Los Alamos HIV Database HIV-1 Env sequences from major subtypes.

Residue	Conservation
Y39	98.9%
F53	99.8%
D62	39.9%
D64	99.7%
H66	99.9%
N67	99.7%
W69	99.8%
H72	96.7%
V75	99.9%
P76	99.9%
D107	99.8%
L111	98.0%
W112	99.7%
K207	99.5%
S209	75.2%
F210	98.3%
P212	99.9%
1213	99.2%
A221	99.4%
W427	99.2%
Y435	99.2%
P437	97.2%
P438	99.6%
M530	99.8%
H564	94.6%
V570	99.7%
W571	99.8%
K574	99.4%
A578	86.0%
W623	99.3%
W628	99.8%
W631	99.8%

Author Manuscript Author Manuscript Author Manuscript Author Manuscript

Supplementary Material

Refer to Web version on PubMed Central for supplementary material.

Acknowledgments

This work was supported by the Center for HIV/AIDS Vaccine Immunology and Immunogen Discovery Grant UM1AI100663 (I.A.W., A.B.W.), NIH HIVRAD Grant P01 AI110657 (I.A.W., J.P.M., A.B.W.), and NIH Grant P50 GM103368 (D.L.). This is manuscript #29422 of The Scripps Research Institute.

References

1. Harrison SC. Viral membrane fusion. Nat Struct Mol Biol. 2008; 15:690–698. [PubMed: 18596815]
2. Lindemann, D., Steffen, I., Pöhlmann, S. Viral Entry into Host Cells. Pöhlmann, Stefan, Simmons, Graham, editors. Springer; New York: 2013. p. 128-149.
3. Lee JH, Ozorowski G, Ward AB. Cryo-EM structure of a native, fully glycosylated, cleaved HIV-1 envelope trimer. Science. 2016; 351:1043. [PubMed: 26941313]
4. Sanders RW, et al. A Next-Generation Cleaved, Soluble HIV-1 Env Trimer, BG505 SOSIP.664 gp140, Expresses Multiple Epitopes for Broadly Neutralizing but Not Non-Neutralizing Antibodies. PLoS Pathog. 2013; 9:e1003618. [PubMed: 24068931]
5. Burton DR, Hangartner L. Broadly Neutralizing Antibodies to HIV and Their Role in Vaccine Design. Annual Review of Immunology. 2016; 34:635–659.
6. Burton DR, Mascola JR. Antibody responses to envelope glycoproteins in HIV-1 infection. Nat Immunol. 2015; 16:571–576. [PubMed: 25988889]
7. Klein F, et al. Antibodies in HIV-1 Vaccine Development and Therapy. Science. 2013; 341:1199. [PubMed: 24031012]
8. West, Anthony P., Jr, et al. Structural Insights on the Role of Antibodies in HIV-1 Vaccine and Therapy. Cell. 2014; 156:633–648. [PubMed: 24529371]
9. Liu J, Bartesaghi A, Borgnia MJ, Sapiro G, Subramaniam S. Molecular architecture of native HIV-1 gp120 trimers. Nature. 2008; 455:109–113. [PubMed: 18668044]
10. Tran EEH, et al. Structural Mechanism of Trimeric HIV-1 Envelope Glycoprotein Activation. PLoS Pathog. 2012; 8:e1002797. [PubMed: 22807678]
11. Kwong PD, et al. Structure of an HIV gp120 envelope glycoprotein in complex with the CD4 receptor and a neutralizing human antibody. Nature. 1998; 393:648–659. [PubMed: 9641677]
12. Guttman M, et al. CD4-Induced Activation in a Soluble HIV-1 Env Trimer. Structure. 2014; 22:974–984. [PubMed: 24931470]
13. Munro JB, et al. Conformational dynamics of single HIV-1 envelope trimers on the surface of native virions. Science. 2014; 346:759. [PubMed: 25298114]
14. Pugach P, et al. A Native-Like SOSIP.664 Trimer Based on an HIV-1 Subtype B env Gene. Journal of Virology. 2015; 89:3380–3395. [PubMed: 25589637]
15. Sanders RW, et al. HIV-1 neutralizing antibodies induced by native-like envelope trimers. Science. 2015; 349
16. Ringe RP, et al. Cleavage strongly influences whether soluble HIV-1 envelope glycoprotein trimers adopt a native-like conformation. Proceedings of the National Academy of Sciences. 2013; 110:18256–18261.
17. Kwon, Y Do, et al. Crystal structure, conformational fixation and entry-related interactions of mature ligand-free HIV-1 Env. Nat Struct Mol Biol. 2015; 22:522–531. [PubMed: 26098315]
18. Finzi A, et al. Topological Layers in the HIV-1 gp120 Inner Domain Regulate gp41 Interaction and CD4-Triggered Conformational Transitions. Molecular Cell. 2010; 37:656–667. [PubMed: 20227370]
19. Myszka DG, et al. Energetics of the HIV gp120-CD4 binding reaction. Proceedings of the National Academy of Sciences. 2000; 97:9026–9031.

Author Manuscript Author Manuscript Author Manuscript Author Manuscript

20. Pancera M, et al. Structure of HIV-1 gp120 with gp41-interactive region reveals layered envelope architecture and basis of conformational mobility. Proceedings of the National Academy of Sciences. 2010; 107:1166–1171.
21. Liu Q, et al. Quaternary contact in the initial interaction of CD4 with the HIV-1 envelope trimer. Nat Struct Mol Biol. 2017; 24:370–378. [PubMed: 28218750]
22. Zhou T, et al. Multidonor Analysis Reveals Structural Elements, Genetic Determinants, and Maturation Pathway for HIV-1 Neutralization by VRC01-Class Antibodies. Immunity. 2013; 39:245–258. [PubMed: 23911655]
23. Zhou T, et al. Structural definition of a conserved neutralization epitope on HIV-1 gp120. Nature. 2007; 445:732–737. [PubMed: 17301785]
24. Wang J, Sen J, Rong L, Caffrey M. Role of the HIV gp120 Conserved Domain 1 in Processing and Viral Entry. The Journal of Biological Chemistry. 2008; 283:32644–32649. [PubMed: 18815131]
25. Anastassopoulou CG, et al. Resistance of a human immunodeficiency virus type 1 isolate to a small molecule CCR5 inhibitor can involve sequence changes in both gp120 and gp41. Virology. 2011; 413:47–59. [PubMed: 21356539]
26. Anastassopoulou CG, Ketas TJ, Klasse PJ, Moore JP. Resistance to CCR5 inhibitors caused by sequence changes in the fusion peptide of HIV-1 gp41. Proceedings of the National Academy of Sciences of the United States of America. 2009; 106:5318–5323. [PubMed: 19289833]
27. Tan Q, et al. Structure of the CCR5 Chemokine Receptor–HIV Entry Inhibitor Maraviroc Complex. Science. 2013; 341:1387. [PubMed: 24030490]
28. Pugach P, et al. A Native-Like SOSIP.664 Trimer Based on an HIV-1 Subtype B env Gene. Journal of Virology. 2015; 89:3380–3395. [PubMed: 25589637]
29. Sanders RW, et al. A Next-Generation Cleaved, Soluble HIV-1 Env Trimer, BG505 SOSIP.664 gp140, Expresses Multiple Epitopes for Broadly Neutralizing but Not Non-Neutralizing Antibodies. PLoS Pathog. 2013; 9:e1003618, 18. [PubMed: 24068931]
30. Carragher B, et al. Leginon: An Automated System for Acquisition of Images from Vitreous Ice Specimens. Journal of Structural Biology. 2000; 132:33–45. [PubMed: 11121305]
31. Potter CS, et al. Leginon: a system for fully automated acquisition of 1000 electron micrographs a day. Ultramicroscopy. 1999; 77:153–161. [PubMed: 10406132]
32. Suloway C, et al. Automated molecular microscopy: The new Leginon system. Journal of Structural Biology. 2005; 151:41–60. [PubMed: 15890530]
33. Zheng SQ, et al. MotionCor2: anisotropic correction of beam-induced motion for improved cryo-electron microscopy. Nature Methods. 2017; 14(4):331–332. [PubMed: 28250466]
34. Zhang K. Gctf: Real-time CTF determination and correction. Journal of Structural Biology. 2016; 193:1–12. [PubMed: 26592709]
35. Voss NR, Yoshioka CK, Radermacher M, Potter CS, Carragher B. DoG Picker and TiltPicker: software tools to facilitate particle selection in single particle electron microscopy. Journal of structural biology. 2009; 166:205–213. [PubMed: 19374019]
36. Ogura T, Iwasaki K, Sato C. Topology representing network enables highly accurate classification of protein images taken by cryo electron-microscope without masking. Journal of Structural Biology. 2003; 143:185–200. [PubMed: 14572474]
37. van Heel M, Harauz G, Orlova EV, Schmidt R, Schatz M. A New Generation of the IMAGIC Image Processing System. Journal of Structural Biology. 1996; 116:17–24. [PubMed: 8742718]
38. Scheres SHW. RELION: Implementation of a Bayesian approach to cryo-EM structure determination. Journal of Structural Biology. 2012; 180:519–530. [PubMed: 23000701]
39. Lyumkis D, et al. Cryo-EM Structure of a Fully Glycosylated Soluble Cleaved HIV-1 Envelope Trimer. Science. 2013; 342:1484. [PubMed: 24179160]
40. Lyumkis D, Brilot AF, Theobald DL, Grigorieff N. Likelihood-based classification of cryo-EM images using FREALIGN. Journal of Structural Biology. 2013; 183:377–388. [PubMed: 23872434]
41. Scheres SHW. A Bayesian View on Cryo-EM Structure Determination. Journal of Molecular Biology. 2012; 415:406–418. [PubMed: 22100448]

Author Manuscript Author Manuscript Author Manuscript Author Manuscript

42. Scheres SHW, et al. Disentangling conformational states of macromolecules in 3D-EM through likelihood optimization. Nat Meth. 2007; 4:27–29.
43. Kirchdoerfer RN, et al. Pre-fusion structure of a human coronavirus spike protein. Nature. 2016; 531:118–121. [PubMed: 26935699]
44. Webb, B., Sali, A. Current Protocols in Bioinformatics. John Wiley & Sons, Inc.; 2002.
45. Pettersen EF, et al. UCSF Chimera—A visualization system for exploratory research and analysis. Journal of Computational Chemistry. 2004; 25:1605–1612. [PubMed: 15264254]
46. DiMaio F, et al. Atomic-accuracy models from 4.5-A cryo-electron microscopy data with density-guided iterative local refinement. Nat Meth. 2015; 12:361–365.
47. DiMaio F, Tyka MD, Baker ML, Chiu W, Baker D. Refinement of Protein Structures into Low-Resolution Density Maps Using Rosetta. Journal of Molecular Biology. 2009; 392:181–190. [PubMed: 19596339]
48. Emsley P, Lohkamp B, Scott WG, Cowtan K. Features and development of Coot. Acta Crystallographica Section D. 2010; 66:486–501.
49. Adams PD, et al. PHENIX: a comprehensive Python-based system for macromolecular structure solution. Acta Crystallographica Section D. 2010; 66:213–221.
50. Lütteke T, von der Lieth CW. pdb-care (PDB CArbohydrate REsidue check): a program to support annotation of complex carbohydrate structures in PDB files. BMC Bioinformatics. 2004; 5:1–6. [PubMed: 14706121]
51. Lütteke T, Frank M, von der Lieth CW. Carbohydrate Structure Suite (CSS): analysis of carbohydrate 3D structures derived from the PDB. Nucleic Acids Research. 2005; 33:D242–D246. [PubMed: 15608187]
52. Barad BA, et al. EMRinger: side chain-directed model and map validation for 3D cryo-electron microscopy. Nat Meth. 2015; 12:943–946.
53. Chen VB, et al. MolProbity: all-atom structure validation for macromolecular crystallography. Acta Crystallographica Section D. 2010; 66:12–21.
54. Schrodinger LLC. The PyMOL Molecular Graphics System, Version 1.8. 2015
55. Krissinel E, Henrick K. Inference of Macromolecular Assemblies from Crystalline State. Journal of Molecular Biology. 2007; 372:774–797. [PubMed: 17681537]

Author Manuscript Author Manuscript Author Manuscript Author Manuscript

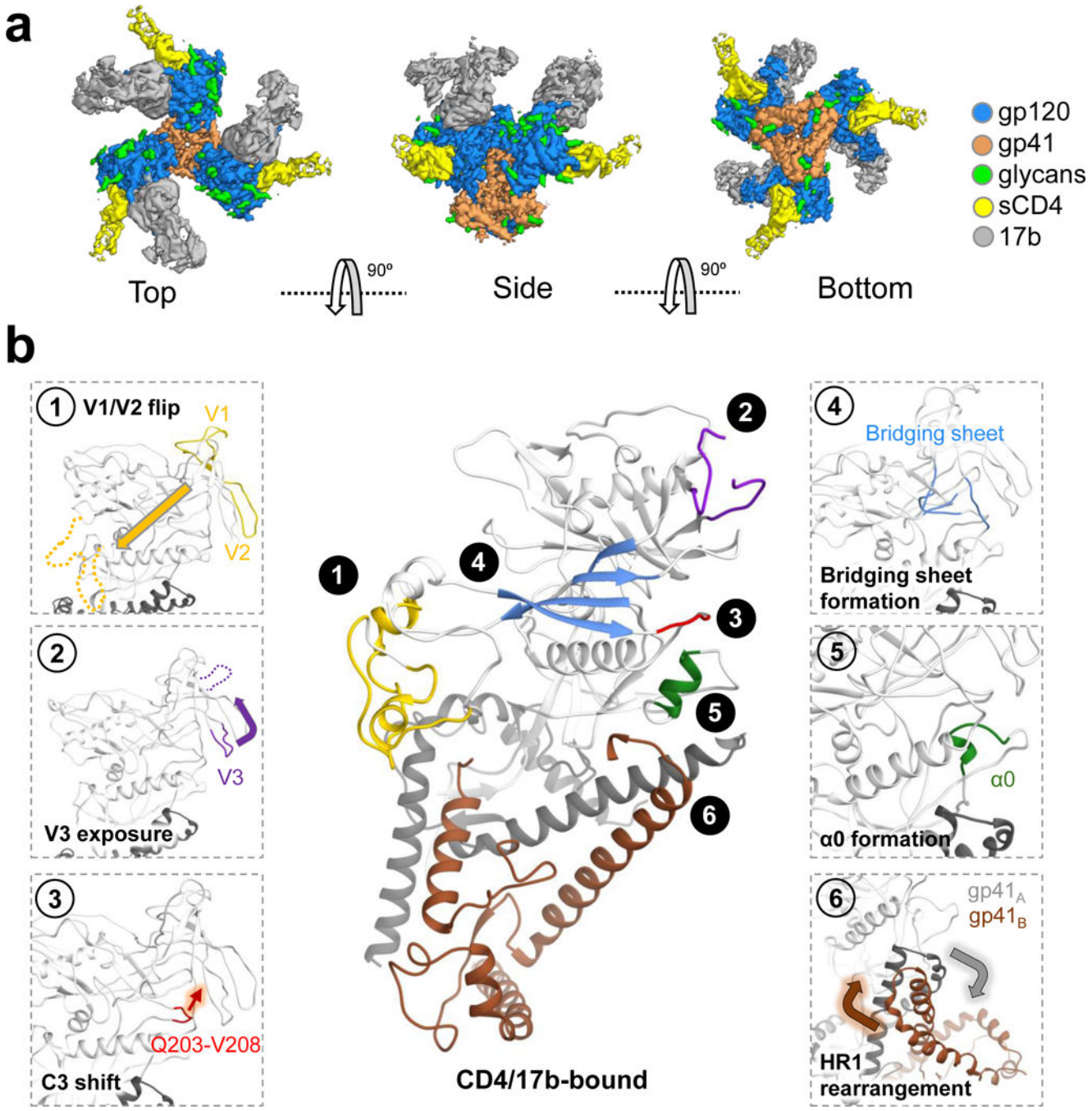

Figure 1. CryoEM reconstruction of B41 SOSIP.664 in complex with sCD4 and 17b Fab

(**a**) CryoEM map segmented by component. (**b**) CD4 binding results in a number of conformational changes in both the gp120 and gp41 regions of Env. Comparison of the CD4/17b-bound (*middle*) to pre-fusion states (*side panels*).

Author Manuscript Author Manuscript Author Manuscript Author Manuscript

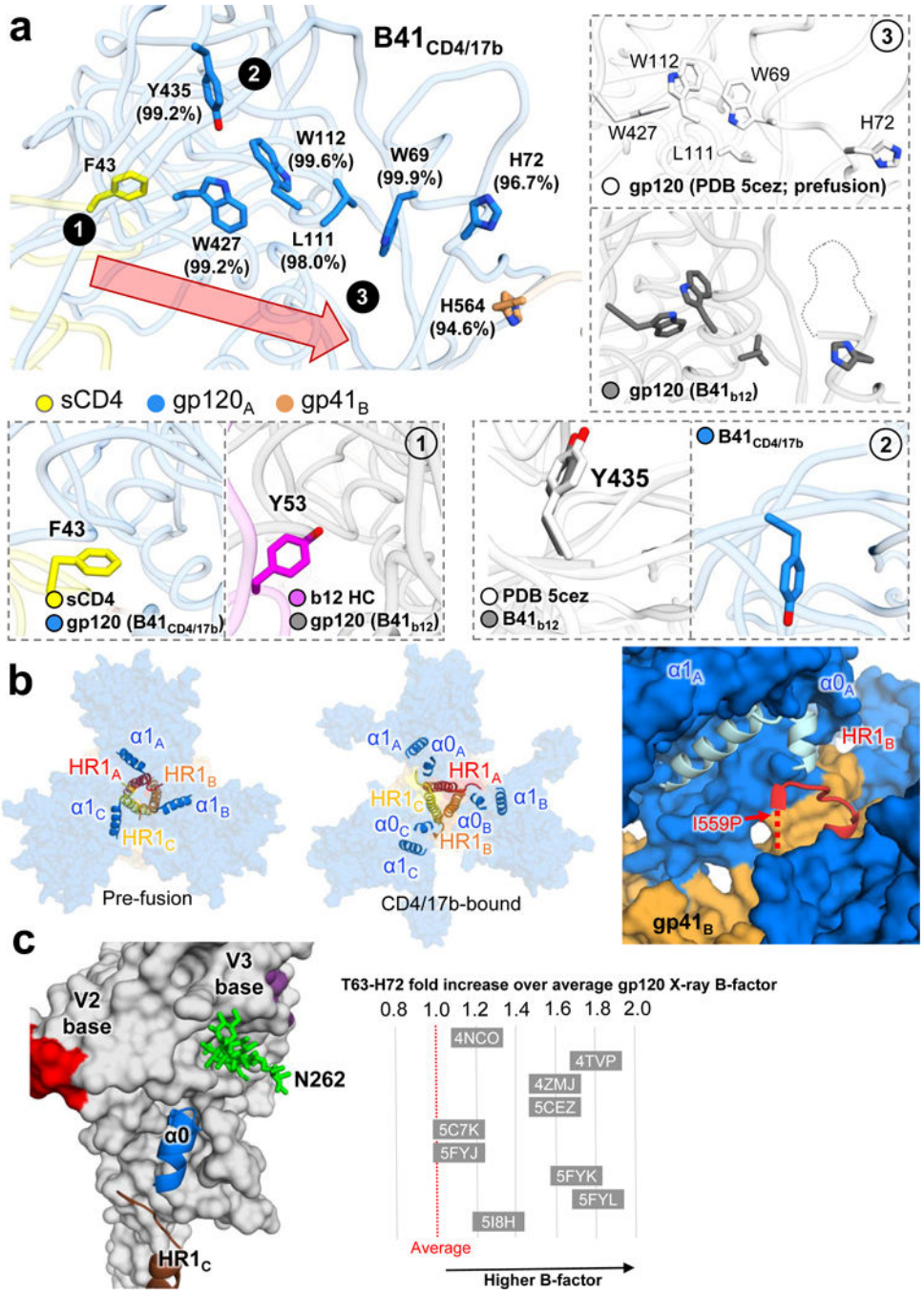

Figure 2. CD4/17b-bound B41 SOSIP.664 structural rearrangements that result in a stable fusion intermediate

(**a**) A network of hydrophobic and aromatic residues transmits the signal upon sCD4 binding that leads to the structural rearrangements in both gp120 and gp41. (**b**) The top of the HR1 helix is capped by the α1 helix of the same protomer in the pre-fusion state (*left*). CD4-binding results in the formation of helix α0, which now caps HR1 of a neighboring protomer (*middle*). A zoom in of the α0-HR1 interaction reveals that it is downstream to the engineered I559P mutation and likely a feature in native Env (*right*). (**c**) The D1 arm of

Author Manuscript Author Manuscript Author Manuscript Author Manuscript

glycan N262 rotates into a newly formed pocket on gp120 (*left*) positioned under the co-receptor binding site at the base of V3, providing a link between the co-receptor binding site and gp41. The α0 helix region is generally disordered in all published crystal structures of SOSIP trimers as evidenced by higher B-factors for this segment relative to the average gp120 value for each structure (*right*).

Author Manuscript Author Manuscript Author Manuscript Author Manuscript

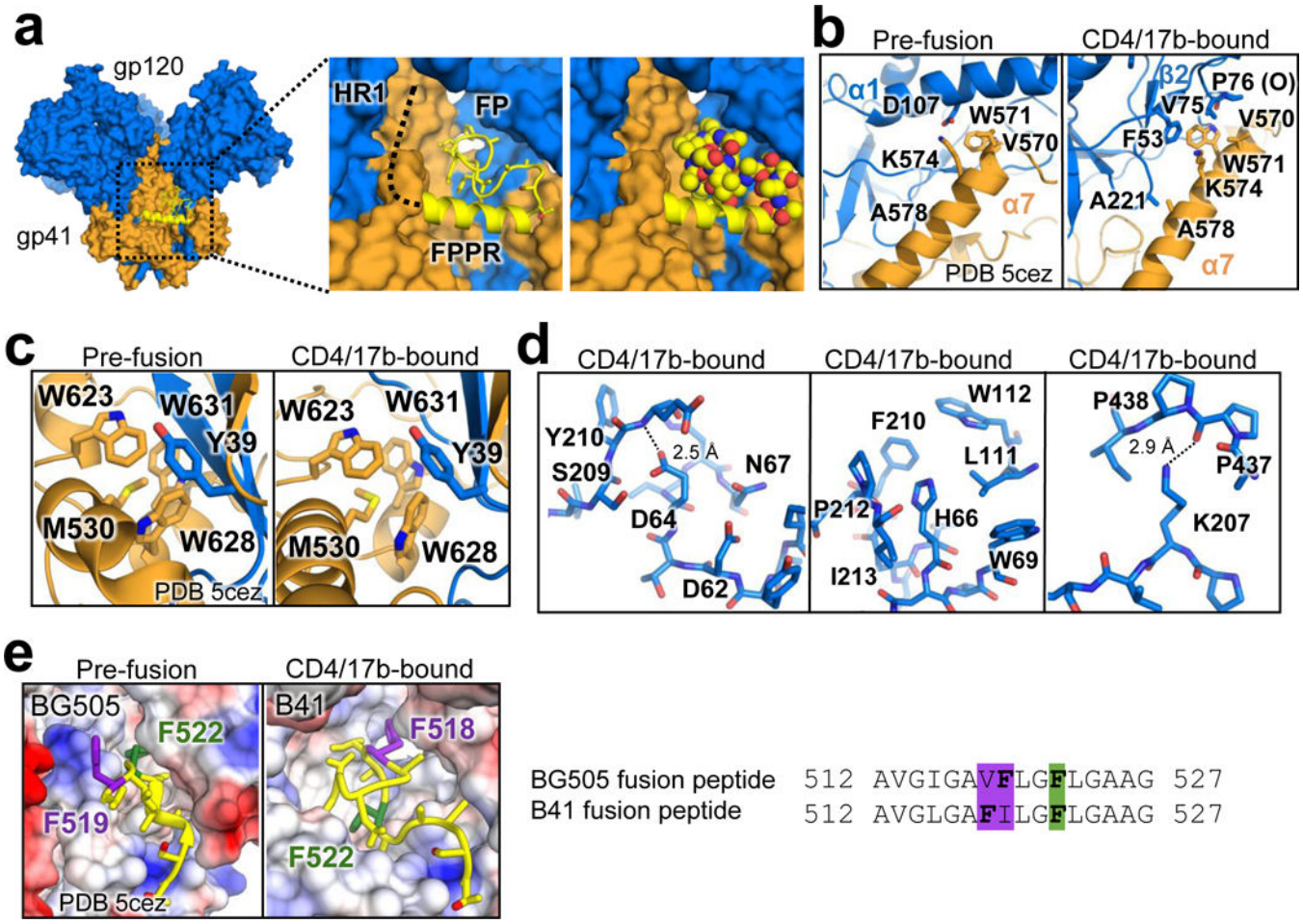

Figure 3. Additional stabilization resulting from CD4-bound rearrangements

(**a**) Space filling model of $B41_{CD4/17b}$ illustrating a newly created pocket that is now occupied by the fusion peptide. A close- up view of the pocket (*center*) and space-filling model (*right*). (**b**) K574 of gp41, which forms a salt bridge with D107 of gp120 in the pre-fusion state, now interacts with F53 of gp120. (**c**) The tryptophan clasp, previously described as a stabilizing feature of the pre-fusion state[14], is retained in the CD4-bound state. (**d**) Intra-protomer stabilizing interactions of helix α0 and β3-β4. (**e**) Two aromatic residues of the fusion peptide rearrange upon CD4-binding and fit in two pockets. Sequence alignment of the fusion peptides of BG505 (pre-fusion) and B41 (CD4-bound) with the aromatic residues highlighted. All pre-fusion model coordinates are based on PDB: 5CEZ.

Author Manuscript Author Manuscript Author Manuscript Author Manuscript

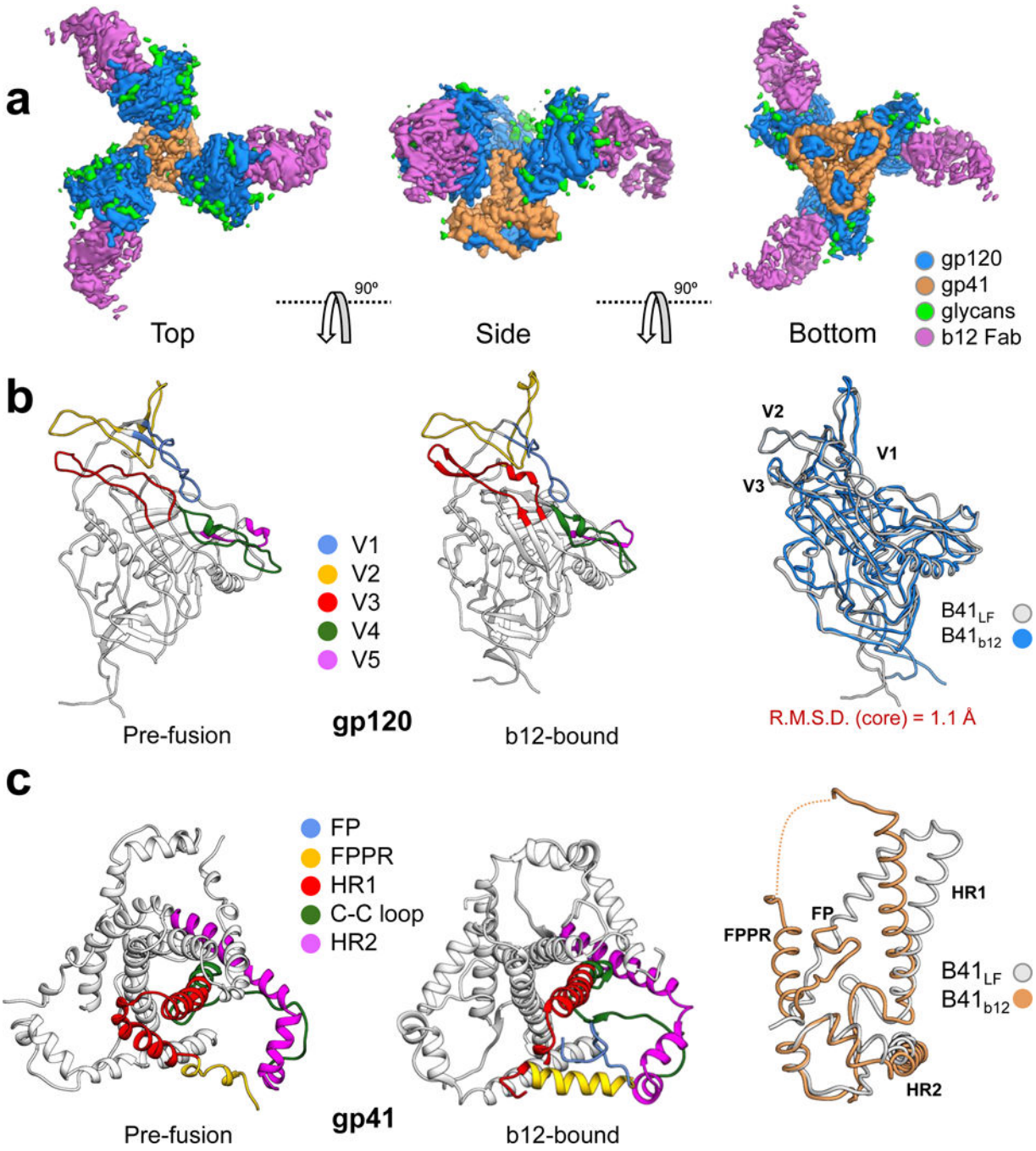

Figure 4. CryoEM reconstruction and model of B41 SOSIP.664 in complex with b12 Fab

(**a**) CryoEM map segmented by component. (**b**) Comparison of gp120 variable loops before and after b12 binding; $B41_{LF}$ (*left*) and $B41_{b12}$ (*middle*). Superposition of gp120 from pre-fusion and b12-bound states reveals only slight structural differences in the individual gp120 subunits (*right*). (**c**) Structural rearrangements in gp41 between the pre-fusion and b12-bound states include repacking of the HR1 three-helix bundle as well as ordering of the fusion peptide and fusion peptide proximal region (FPPR). Alignment onto HR2 of single

gp41 chains from $B41_{LF}$ and $B41_{b12}$ reveals a relative translocation of HR1 and rearrangement of the FP and FPPR (*right*).

Author Manuscript Author Manuscript Author Manuscript Author Manuscript